Journal of Low Temperature Physics
https://doi.org/10.1007/s10909-019-02312-5

# Thermal Crosstalk Measurements and Simulations for an X-ray Microcalorimeter Array

**Antoine R. Miniussi[1,2] · Joseph S. Adams[1,2] · Simon R. Bandler[1] · Sophie Beaumont[1,2] · Meng P. Chang[1,3] · James A. Chervenak[1] · Fred M. Finkbeiner[1,4] · Jong Y. Ha[1,5] · Ruslan Hummatov[1,2] · Richard L. Kelley[1] · Caroline A. Kilbourne[1] · Frederick S. Porter[1] · John E. Sadleir[1] · Kazuhiro Sakai[1,2] · Stephen J. Smith[1,2] · Nicholas A. Wakeham[1,2] · Edward J. Wassell[1,3]**

Received: 20 August 2019 / Accepted: 11 December 2019


**Abstract**
Arrays of high-density microcalorimeters require careful heat sinking in order to minimize the thermal crosstalk between nearby pixels. For the array of microcalorimeters developed for the Athena X-ray Integral Field Unit instrument, which has more than 3000 pixels on a 275 μm pitch, it is essential to address this problem in order to meet the energy-resolution requirements. The instrument's energy-resolution budget requires that the impact of the thermal crosstalk on the energy resolution be a contribution that, added in quadrature to other energy-resolution contributions, is less than 0.2 eV. This value results in a derived requirement that the ratio between the amplitude of the crosstalk signal to an X-ray pulse (for example at 6 keV) is less than $1\times10^{-3}$ (for the first neighbor), less than $4\times10^{-4}$ (for the diagonal neighbor) and less than $8\times10^{-5}$ (for the second nearest neighbor). We have measured the thermal crosstalk levels between pixels in various geometries and configurations. The results show a crosstalk ratio which is at least a factor of 4 lower than the derived requirement. We also developed a finite element (FEM) 2D thermal model to predict the thermal behavior of large-scale arrays. This model successfully simulates the measured data in terms of pulse amplitude and time constants.

**Keywords** Thermal crosstalk · TES · Athena/X-IFU · FEM

✉ Antoine R. Miniussi
antoine.r.miniussi@nasa.gov

[1] NASA Goddard Space Flight Center, Greenbelt, USA

[2] CRESST II – University of Maryland Baltimore County, Baltimore, USA

[3] SSAI Science Systems and Applications, Inc., Lanham, USA

[4] Sigma Space Corp., Lanham, USA

[5] SB Microsystems, Glen Burnie, USA

Published online: 18 January 2020

## 1 Introduction

We have been developing superconducting transition-edge sensor (TES) microcalorimeters for a variety of potential astrophysics missions, including Athena [1]. The X-ray Integral Field Unit (X-IFU) [2] instrument on this mission includes a high-density kilo-pixel array on a 275 μm pitch. This close-packed configuration induces electrical and thermal crosstalk between nearby pixels [3]. The Athena/X-IFU mission has an energy-resolution budget allocation of 0.2 eV for thermal crosstalk, which is added to other energy-resolution limiting terms in quadrature. This leads to a derived requirement on the crosstalk ratios between the amplitudes of the crosstalk signal and an X-ray pulse (e.g., at 6 keV) that is less than $1\times10^{-3}$ (first neighbor), $4\times10^{-4}$ (diagonal neighbor) and $8\times10^{-5}$ (second nearest neighbor). The initial budget allocation and the derived crosstalk requirements are based on Iyomoto et al. [3].

We have measured the thermal crosstalk on several configurations within arrays of microcalorimeters and developed a numerical model to predict the thermal behavior of future designs. In this publication, we describe the experimental measurements taken at NASA/GSFC for different designs and features of $8\times8$ arrays of TES microcalorimeters. The results are compared with a 2D finite element thermal model developed to predict the thermal behavior of large-scale arrays.

## 2 Crosstalk Measurement

### 2.1 TES Design and Experimental Setup

The X-ray microcalorimeter is composed of many elements, but only the main features relevant to this study are described and represented in the schematic in Fig. 1, left. The superconducting bilayer TES consisting of Mo/Au is overhung by a Bi/Au absorber which absorbs and converts the energy of incoming X-ray

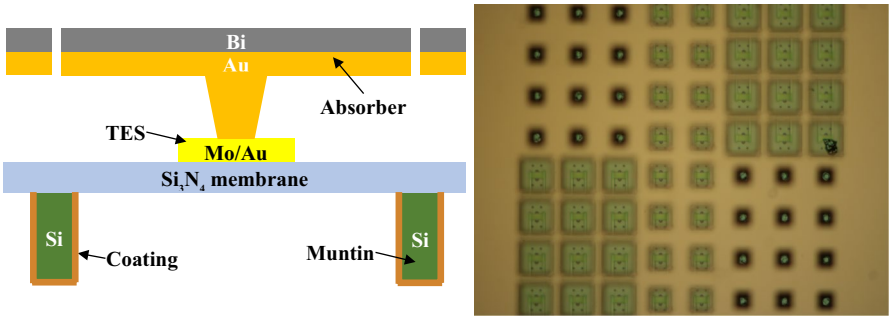


**Fig. 1** Left: schematic of a TES microcalorimeter. The absorber is on top, just below the TES, resting on the SiN membrane supported by the Si muntins. Many elements are not represented such as the Nb leads. Right: picture taken from below one of the arrays tested that has five different muntin widths. We can see the TES through the transparent SiN membrane (Color figure online)

energy into heat. Each pixel is supported by a 0.5-μm-thick SiN membrane, lying on a grid of 300-μm-thick Si muntins shaped by back-etching under each TES to provide a weak thermal link to the bath. The whole chip is thermalized to the bath through gold wire-bonds connected on the top surface of the silicon area surrounding the array. A coating of Cu or Au is added only to the sides and bottom of the muntins in the Si grid region of the pixels to increase the thermal conductivity between the chip and the bath.

Two chips have been tested, covering several different configurations. Chip A has five different muntin widths of 42 μm, 77 μm, 112 μm, 130.5 μm and 149 μm. A photograph of the bottom surface of this chip is shown in Fig. 1, right. Chip B is a more uniform chip with muntin widths of 112 μm and 105 μm on the orthogonal direction. For both chips, the TESs are 75 μm long and 37.5 μm wide for an aspect ratio of 1:0.5 [4].

For chip A, only the crosstalk between TESs with muntin widths of 42, 77 and 112 μm has been measured since the TES with larger muntin widths did not yield properly. Chip B provided a second measurement at 112 μm and one at 105 μm. Chip B was tested both with and without the addition of a Cu layer on the bottom side of the muntins.

All the experiments used a bath temperature of 55 mK. All the measurements were carried out with the TESs biased at 10% of the TES normal resistance. We used an $^{55}$Fe source emitting MnK X-rays at 6 keV.

### 2.2 Data Processing

Each measurement of crosstalk between pairs of pixels simultaneously operated used the same data acquisition and processing. We call the microcalorimeter in which the X-ray is absorbed the "source," and the studied detector the "receiver." (1) The data acquisition for both pixels is triggered by the *source* hit by MnK X-ray at 6 keV; (2) the data from both the *source* and the *receiver* signals are stored for each X-ray event detected in the *source* with a total of more than 4000 counts in each dataset; (3) different datasets are recorded for both positive and negative bias points of the *receiver* pixel to remove by subtraction the electrical crosstalk generated by the SQUID readout, the bias circuit and the wires [5]; (4) MnK X-ray pulse at 6 keV is recorded for the *receiver* at the same bias point.

The amplitude of the thermal crosstalk pulse on the *receiver* is measured by averaging 20 points around the maximum of the pulse after removing electrical crosstalk. The X-ray pulse is an average of only 6 keV pulses on the *receiver*. To discard the effect of the nonlinearity of the TES, the decay of the pulse is fit with a single exponential (see dashed black line in Fig. 2, left). We introduce a figure of merit, the crosstalk ratio $f$ defined as $f = \frac{h_{\text{crosstalk}}}{h_{6\,\text{keV}}}$ with $h_{\text{crosstalk}}$, the amplitude of the crosstalk pulse and $h_{6\,\text{keV}}$ the amplitude of the 6 keV pulse on the *receiver*. The rising and decreasing parts of the crosstalk pulse are fit separately with a single exponential equation, as shown in Fig. 2, right.

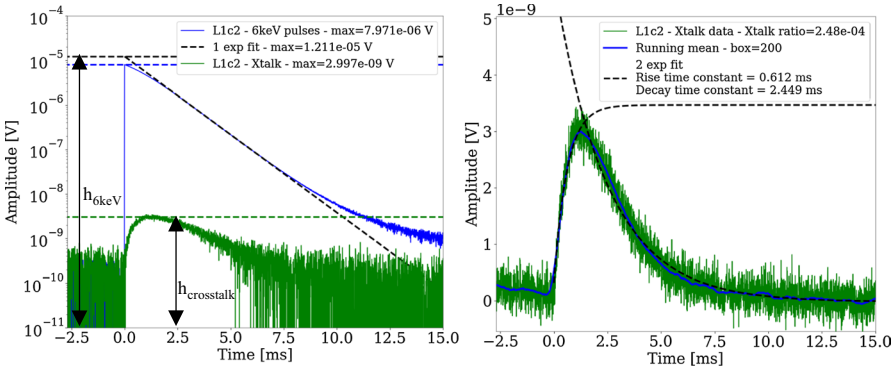


**Fig. 2** An example of a crosstalk measurement is presented here. Left: this graph shows a comparison between the 6 keV X-ray signal and the crosstalk signal on the *receiver*. Both traces are the average of the recorded events. The impact of the nonlinear transition is clear from a comparison of the data to a single exponential fit. The *y*-axis is on a logarithmic scale. Right: zoom-in of the average *receiver* crosstalk pulse-shape. The average pulse is in green, while the blue line is a running mean over 200 points. The rise and decay slopes are each fit with a single exponential (Color figure online)

## 2.3 Experimental Results

For the case of nearest neighbors (one pixel apart), we measured crosstalk ratios of $2.3\times10^{-4}$ for the smallest 42 µm muntin width to $1.3\times10^{-4}$ for the largest 112 µm one. The experimental data are plotted in circles in Fig. 3, left. The values, although stable for repetitive measurements on the same *source* and *receiver*, fluctuate over a

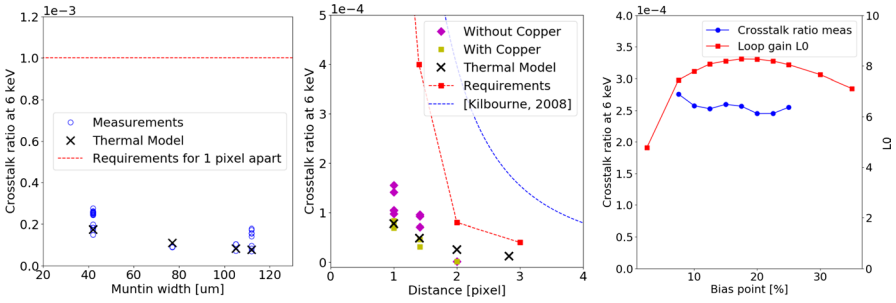


**Fig. 3** Left: nearest neighbor crosstalk ratio measurements for different muntin widths (42, 77, 105 and 112 µm). The crosstalk increases for smaller muntin widths. The data are compared with the requirement of $1\times10^{-3}$ (dashed line) for nearest neighbor crosstalk. The results from a thermal model are represented as black crosses. Middle: crosstalk ratio measurements for 1, 1.4 (diagonal) and 2 pixels apart for a muntin width of 112 µm. The additional Cu layer on the Si muntins decreases the crosstalk. Measurement for 2 pixels apart is below the measurement noise threshold of the receiver. The results from a thermal model for the case with copper are represented as black crosses. The results are also compared with previous measurements by Kilbourne (taken from [6]). The muntin in that case was 70 µm wide. Right: crosstalk ratios for TES bias from 7.5 to 25% (left axis) and measured loop gain $L_0$ for bias points between 2.5 and 35% (right axis). At the bias points used for the measurements, $L_0$ varies from 7.6 to 8.1. These measurements have been carried out for *source*/*receiver* separated by a 42-µm muntin (Color figure online)

given muntin width for different pixel pairs. Further measurements are ongoing, and the first results showed a potential correlation between the thermal crosstalk and the number of superconducting TES wires between the two studied TES. However, the results show that the crosstalk increases with narrower muntins. This is explained by the direct impact of the width on the thermal conductance of the muntins defined as $G_{\text{muntin}} = \lambda \frac{S}{L} \Delta T$ in W/K, with $\lambda$ the thermal conductivity in W/m K, $S$ the cross-sectional area of the muntin in m$^2$, $L$ its thickness in m and $\Delta T$ the temperature difference between the two studied elements in K. Widening the muntin by a factor 2 leads to increase the thermal path toward the heat sink and reduce the crosstalk by the same factor as we see in the measured data.

To understand the impact of the additional copper layer on the backside of the chip, we carried out two measurements on chip B before and after adding a layer of 2.67 µm of Cu on the bottom of the Si muntins and its sides up to 80% of the height. We compared these results for different distances between the *source* and the *receiver* as shown in Fig. 3, middle. For the nearest neighbor case and the nearby diagonal pixel, the crosstalk ratio $f$ for the case without copper is $1.2 \times 10^{-4}$ and $8.0 \times 10^{-5}$, respectively. With the addition of copper, which increases the thermal conductivity of the system, $f$ decreases by a factor 2 for both geometries. The difference in crosstalk for 2 pixels apart cannot be determined as the crosstalk is so low that it was not possible to measure it. This data can be compared with the X-IFU requirements, based on Iyomoto et al. [3] measurements and previous measurement taken by Kilbourne et al. [6]. The crosstalk fraction we measured is a factor 4 and 10 lower compared with these two sets of data, respectively. The higher crosstalk ratios previously measured are explained by two mains factors: (1) a stronger thermal link between the pixel and the bath (higher $G_{\text{bath}}$): 150 pW/K for Iyomoto and 234 pW/K for Kilbourne; (2) a smaller muntin width: 50 µm for Iyomoto and 70 µm for Kilbourne.

Finally, we have also measured the variation of crosstalk ratio for different bias points from 7.5 to 25% of the transition (see Fig. 3, right). After correcting the measurements to remove the effect of the nonlinear transition, we observe that the ratio is stable over the whole range of bias points to within 5%. The amount of crosstalk also highly depends on the electro-thermal feedback (ETF) [7] which removes part of the deposited energy on the *source* pixel by change in joule power. The residual energy in the pixel after the ETF effect is function of $1/(1+L_0)$ with $L_0$ the loop gain defined as:

$$L_0 = \frac{\alpha I_0^2 R_0}{T_0 G_{\text{bath}}} \frac{R_0 - R_{\text{s}}}{(1+\beta)R_0 + R_{\text{s}}}$$

with $\alpha = \frac{T}{R}\frac{\partial R}{\partial T}\Big|_I$ and $\beta = \frac{I}{R}\frac{\partial R}{\partial I}\Big|_T$ the temperature and current sensitivities of the TES, $R_0$, $I_0$, $T_0$ the resistance, current and temperature of the TES, respectively, $R_{\text{s}}$ the shunt resistance of the circuit and $G_{\text{bath}}$ the thermal conductance between the TES and the bath temperature in W/K. However, the measurements of the loop gain $L_0$ [8] on our TES show only a small variation (see Fig. 3, right) for this range of bias point. With values between 7.6 and 8.1, the variation of loop gain is not strong enough to modify the response of the TES.

## 3 Numerical Model

### 3.1 Description

A numerical thermal model has been developed to understand thermal crosstalk and predict the impact of future changes to the TES microcalorimeter array design. The model was developed in 2D using finite element software COMSOL Multiphysics [9]. Five blocks are modeled (see Fig. 4, left), representing the dominating thermal elements of the TES array: the pixel (TES + absorber), the Si substrate, the Cu coating separated into a phonon and an electron block and finally the heat sink at 55 mK. The impact of the SiN membrane on top of the silicon is not included here as it adds computing time and impacts the results by less than 0.5%.

The ETF is implemented in the model through the loop gain, by considering the residual energy $E_{\text{residual}} = E_{6\,\text{keV}} \frac{1}{1+L_0}$, after the effect of the ETF is applied to the whole *source* pixel.

Since the crosstalk measurement for a muntin width of 112 µm gives the same result for the non-uniform chip A and the uniform chip B, we developed the model for a uniform width of muntin. The parameters $C_{\text{pixel}}$ and $G_{\text{bath}}$ are constrained as they result from measurements. The following parameters have a high impact on the result and are left floating: $G_{\text{e-p\_Cu}}$ (thermal conductance of the electron–phonon coupling of the copper coating), $G_{\text{kap\_Si-Cu}}$ (thermal conductance of the Kapitza resistance between Si and Cu) and $G_{\text{wb}}$ (thermal conductance of the wire bonding). All the values stay within the error bars observed in the literature.

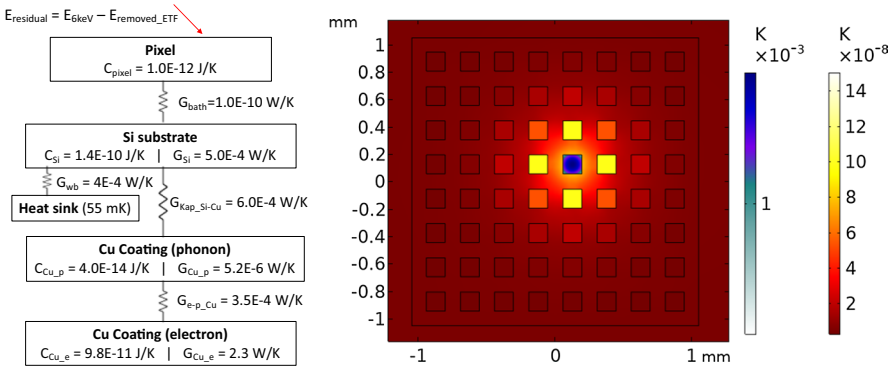


**Fig. 4** Left: block diagram of the thermal circuit used to model the crosstalk performance with the main parameters used for the numerical model. The values for $C_{\text{pixel}}$ and $G_{\text{bath}}$ values were measured experimentally, and the others are estimated. Right: this is a simulated thermal image of the pixel array with an X-ray pulse heating the *source* pixel (blue scale) and the heat wave flowing to the nearby *receiver* pixels (red scale). The amplitude of the *source* pixel is 1 mK, while the receivers heat up by as much as 0.1 µK (Color figure online)

### 3.2 Comparison of the Model with Experimental Data

The numerical thermal model is run for all the cases studied above with the parameters given in Fig. 4, left and a loop gain $L_0 = 8$ resulting from complex impedance measurement [8] on chip A for a bias point of 10%. The results from the model are compared to the experimental data in Fig. 3, left and middle and Fig. 5. The model shows a good agreement in terms of the crosstalk ratio $f$, with a maximum error of 20% for the case where the average measured values were for muntin widths of 42 and 112 µm. The shape of the modeled crosstalk pulses (Fig. 5) also agrees well with the measured ones, with a maximum error of 20% on the rising (~0.7 ms) and decay (~2.5 ms) time constants.

### 3.3 Crosstalk Simulation for X-IFU Array

We also have simulated the thermal crosstalk for an X-IFU like array. As the thermal characteristics and the design are not fully defined yet, we used the current requirement values with: $G_{\text{bath}} = 72$ pW/K, $C_{\text{pixel}} = 0.73$ pJ/K, $\text{TES}_{\text{size}} = 75$ µm, $L_0 = 6$. The TES pitch is increased to 275 µm, and the muntin width is set at 100 µm. The thickness of the Au coating is defined at 2 µm. Further modeling will be required when the features of the X-IFU array will be finalized.

The results (Fig. 6) show a similar impact as the small array studied in this article, with a crosstalk ratio a factor 3–11 below the requirements depending on the distance and similar rise and decay time constants.

## 4 Conclusion

We have measured the crosstalk ratio and the thermal rise and decay time constant for several muntin width configurations as well as a comparison of crosstalk with and without the addition of a copper coating on the bottom surface and sidewalls of the muntins. These results show that this design generates a crosstalk 4 times lower than

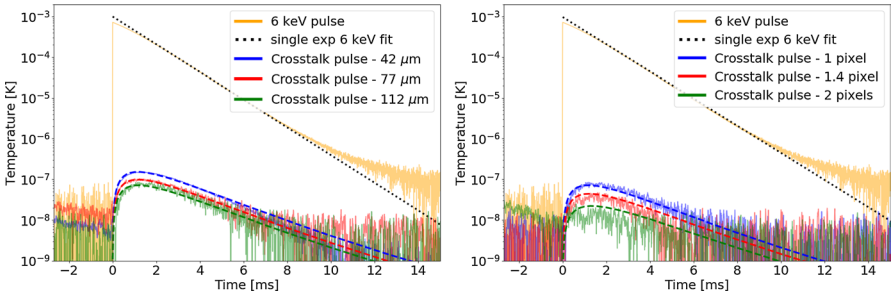


**Fig. 5** Comparison between measurements (solid line) and thermal modeling (dashed line) for three different muntin widths (right) and three distances (left). The dotted line represents the fitted measured 6 keV pulse. The measured data, in nV, are normalized in order to determine the maximum of the fitted 6 keV pulse at 1 mK (Color figure online)

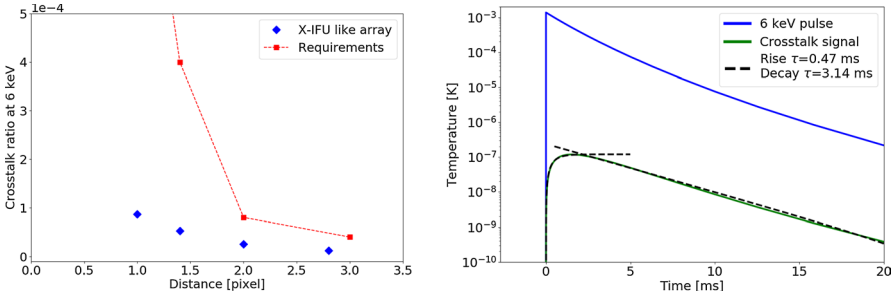


**Fig. 6** Result of the numerical model for a potential X-IFU array design. Left: crosstalk ratio $f$ for different distances between *source* and *receiver*. Right: 6 keV pulse and crosstalk signal timelines. The rise and decay time constants of the crosstalk signal are fitted separately with a single exponential (Color figure online)

the requirements stated by Athena/X-IFU. The change in muntin width largely impacts the results with larger muntin width leading to smaller crosstalk. Adding a layer of Cu on the backside of the muntins improves the crosstalk by a factor 2 for these small $8\times8$ chips and may have an even greater impact in larger arrays. We have successfully modeled the thermal behavior in terms of amplitude and time constants of the source and the receiver pixels for all the measured configurations.

We used this model to simulate the expected crosstalk ratio for one of the TES array designs proposed for Athena/X-IFU. It shows a level of crosstalk between pixels 3–11 times lower than the requirement depending on the distance between the *source* and the *receiver*.

The next step to this work is to calculate the impact on the energy resolution of this thermal crosstalk and compare it with the requirement of a maximum budget of 0.2 eV dedicated to the thermal crosstalk.

A more detailed study will be published in the near future to assess the observed variations of thermal crosstalk between pixels and the hypothesis that it is correlated with the number of superconducting TES wires.

## References


1. K. Nandra et al. (2013) arXiv:1306.2307 [astro-ph.HE]
2. D. Barret et al., *Proceedings, SPIE Space Telescopes and Instrumentation 2014: Ultraviolet to Gamma Ray*, vol. 9905, p. 99052F (2016). https://doi.org/10.1117/12.2232432
3. N. Iyomoto et al., IEEE Trans. Appl. Superconduct. **19**(3), 557–560 (2009). https://doi.org/10.1109/TASC.2009.2017704
4. K. Sakai et al., Pixel optimization of Mo/Au bilayer transition-edge sensors for AC-biased readout. J. Low Temp. Phys. This special issue LTD18 (2019)
5. N. Iyomoto et al., J. Low Temp. Phys. **151**(1–2), 506 (2008). https://doi.org/10.1007/s10909-007-9682-5
6. C. Kilbourne et al., *Proceedings, SPIE Space Telescopes and Instrumentation 2008: Ultraviolet to Gamma Ray*, vol. 7011, p. 701104 (2008). https://doi.org/10.1117/12.790027
7. K.D. Irwin et al., Appl. Phys. Lett. **69**, 1945 (1996). https://doi.org/10.1063/1.117630
8. T. Saab et al., Nucl. Instrum. Methods Phys. Res. A **559**, 712 (2006). https://doi.org/10.1016/j.nima.2005.12.112
9. COMSOL Multiphysics, v. 5.4. www.comsol.com, COMSOL AB, Stockholm, Sweden